Active phase locking of a tiled two-grating assembly for high-energy laser pulse compression using simultaneous controls from far-field profiles and interferometry

A. K. Sharma[1,2] · A. S. Joshi[1] · P. A. Naik[1,2] · P. D. Gupta[1,2]

Abstract A prototype study on active phase locking of a tiled two-grating assembly (TTGA) using four electronic nanometric actuators has been reported, for its use in high-energy laser pulse compression. Measurement and correction of various phase errors of a TTGA have been demonstrated with a precision of sub-50 nm in differential longitudinal translational and sub-10 μrad in differential angular errors using controls derived from simultaneous recording of laser interferogram and far-field profiles of reflected and diffracted beams from TTGA differentiating in-plane rotation with respect to tip error, which is otherwise difficult in the case of using interferometry alone. Multiple-level intensities in the thresholds of the power spectra of apodized interferogram and far-field profiles have been adapted to estimate spatial frequencies and beam peak positions with sub-pixel accuracies.

1 Introduction

Chirped pulse amplification (CPA)-based high-energy high-power ultra-short pulse-laser systems [1] are required to study physical processes involved in laser–plasma interaction [2], generating secondary sources of radiation, charged and neutral particles [3–6] for various applications. Energy or power scaling of any CPA-based laser system [1] is often limited by the size and damage threshold of the pulse compression gratings. Due to less availability of large size gratings, two or more gratings are phased in such a way that a tiled grating assembly (TGA) mimic a monolithic grating [7–22]. Two or more such tiled grating assemblies are used to build a laser-pulse compressor for large size, chirped laser beam, to achieve high-energy ultra-short laser pulses. For example, three small size gratings [14 cm (length)×12 cm (width)×2 cm (thickness) from M/s Spectrogon, UK] are used in one grating assembly and three such tiled grating assemblies have been incorporated in the pulse compressor of a 50 TW class hybrid Nd:glass laser system [23, 24] at RRCAT Indore.

Grating with large size and adequate specifications are difficult to fabricate due to technological challenges and hence their cost is also very high. For instance, maintaining wave front quality of a diffracted beam over larger aperture, one would require a thicker grating substrate with smaller thermal expansion coefficients and smaller groove density errors leading to a larger weight of gratings and difficult fabrication process respectively. Next, use of single monolithic grating of larger size also poses challenges in their handling and require additional mechanical tools. Smaller size gratings are easier to handle and to maintain wavefront quality of diffracted beam in a tiled grating assembly. Further, small errors in the groove density of the tiled gratings can also be compensated with differential angle of incidence. But TGA's shall require additional diagnostics and correction setups to estimate and correct various phase errors as discussed in the next paragraph.

There are several types of phase errors e.g. angular tip, tilt and in-plane rotation and longitudinal, lateral translation in any tiled optical assembly, wherein one optic is fixed relative to others. In case of TGA, there could be inter-grating groove density errors that also need to be addressed for phase locking of TGA for laser pulse compression. Several methods have been reported in the

✉ A. K. Sharma
aksharma@rrcat.gov.in

1 Raja Ramanna Centre for Advanced Technology, Indore 452013, India

2 Homi Bhabha National Institute, Mumbai 400094, India

literature to measure and correct these errors. For example, diagnostics based on analysis of far-field intensity distribution [10, 11, 20–22] of reflected and/ or diffracted light from a tiled optical system, and two-dimensional interferometry [8, 9, 13–18] both either using single or two laser wavelengths. Both these methods are simple and sensitive for the detection of various phase errors but have their own advantages and disadvantages.

In case of tiled grating assembly, any difference in the groove density of the two gratings for given angle of incidence shall result in different diffraction angles for beamlets from phase-locked TGA. Such situation can also occur for two gratings of identical groove density for different angles of incidences, i.e. differential angle of incidence error or tilt error. Therefore, it is difficult to differentiate tilt error with groove density error from measured angles of diffraction for beamlets from TGA. Likewise, it is difficult to avoid ambiguity between tip errors with in-plane rotation error and longitudinal piston with lateral piston of tiled grating assembly using interferogram alone, recorded using diffracted and a reference beam, which is used to generate three actuation controls namely tip, tilt and piston. In general, the lateral piston also affects the focal spot intensity distribution [17] but has no angular wavelength dependence and hence no separate control is required for lateral piston in the case of tiled pulse compressor.

In contrast, simultaneous monitoring of far-field beam profiles of reflected and diffracted beam from TTGA, the mismatch between angle of reflection and diffraction and plane of reflection and diffraction can easily be differentiated. Once plane of reflection and diffraction are matched, observing focal spot splitting (or modulation in the far-field beam profile) of otherwise single focal spot of the reflected and diffracted beam one can obtain information on groove density error of tiled gratings. However, in the case of focal spot-based diagnostics alone deriving various controls for tip, tilt, in-plane rotation and piston is also very challenging and difficult as focal spot distribution is quite complicated in simultaneous presence of various phase errors in the tiled grating assembly [25, 26]. Next, focal spot intensity distribution gets further complicated in the presence of beam wave front distortions and for a spectrally broadband high-power pulsed laser beam. However, one may use far-field focal spot-based diagnostics to phase lock a tiled grating assembly using global optimization of various errors in such a way that one achieve single focal spot in diffracted and reflected beam but shall require a difficult algorithm and that is quite challenging due to complicated far-field laser profile of a high-power laser beam. In contrast, a low-power monochromatic beam may be used in far-field diagnostics to avoid errors due to beam aberrations of the high-power laser beam.

It is clear from the above discussion that estimating various beam angles from either method and hence the phase errors of TGA is one of the key requirements to achieve a phase-locked TGA with sub wavelength accuracies. Using laser interferogram recorded between a reference and diffracted beam from TGA, one estimate diffracted beam cross-over angles with respect to a reference beam either by directly estimating fringe spacing and orientation or estimating spatial carrier frequencies of the two halves of the interferogram. Therefore, in order to have correct actuation controls for alignment of tiled gratings assembly, it is important to know the magnitude and sign of beam angles relative to the reference beam. The piston error is estimated by analyzing two halves of the interferogram and analyzing the intensity distribution of far-field profiles.

In the case of estimating tip and tilt errors using spatial frequencies of the interferogram, the accuracies of phase errors directly depend on accuracies in the estimation of spatial carrier frequency [27–31] and is limited, especially in the case when the spatial carrier frequencies are not integral or half integral multiples of the frequency interval dictated by the total number and size of pixel of CCD used to record the interferogram. Further, the presence of systematic or non-systematic noises in the interferogram also affect the estimation of the spatial carrier frequencies. To improve the accuracies in estimating of peak positions of far-field profiles and spatial carrier frequencies, multiple-level thresholds. of far-field intensity distribution and power spectrum of apodized interferogram with suitable padding have been adapted leading to sub-pixel accuracies in the estimation of a peak spatial carrier frequencies of an interferogram and peak positions of far-field profiles (hence beam angles) below diffraction-limited resolution [10], respectively. Apodization of an interferogram helps to reduce picket fence effects and suppress frequencies generated due to finite-size interferogram. The peak spatial frequencies are estimated as intensity-weighted function of thresholded and apodized power spectra.

To address ambiguities in paired variables of TGA, a four-control variable hybrid scheme, comprising a three-control variables from laser interferometry and one-control variable from a far-field diagnostics involving simultaneous monitoring of reflected, diffracted and reference beams, is implemented in prototype study of tiled two gratings assembly (TTGA). While phase-error correction in a tiled grating assembly may be achieved using manual controls, an active electronic-error correction system will be useful to minimize errors, reduce maintenance time and to keep tiled grating assembly phase locked on a long-term basis. This paper presents theoretical and experimental studies on a prototype of a four-variable, automated phase control of tiled two-grating assembly (TTGA) with a worst-case precision of sub-50 nm in differential piston and sub-10 µrad

in differential tip, tilt and in-plane rotation. A monochromatic light source at wavelength (λ) of 632.8 nm with full angle divergence of ~16 µrad has been used in the present experimental studies on phase locking of TTGA. Long-term stability of a TTGA has been demonstrated over 1 h. Using detailed analysis of far-field intensity distribution, one achieves actuator-limited angular precision of ~1 µrad in tip, tilt and in-plane rotation errors.

2 Theoretical background

To obtain intensity distribution of an interference pattern for a two-beam laser interferometry, in an interaction geometry shown in Fig. 1a, one first defines a Gaussian beam with electric field E(x,y,z), as

$$E(\text{x,y,z}) = E_o \left(\frac{W_0}{W(z)} \right) e^{-\frac{(x^2+y^2)}{W(z)^2}} e^{-j[kz+k\frac{(x^2+y^2)}{2R(z)}-\tan^{-1}\frac{z}{Z_R}]} \quad (1)$$

where k ($=2\pi/\lambda$ is the propagation constant, $W(z)$ [$=W_o\{1+(z/z_R)^2\}^{1/2}$] is the beam waist at distance z, and $R(z)$ ($=z+Z_R^2/z$) is the curvature of phase front at distance z, and
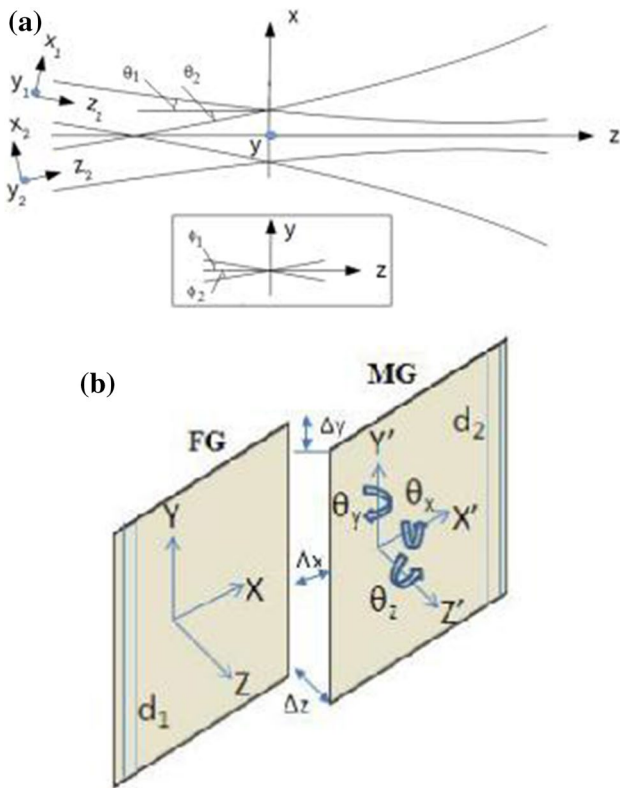

Fig. 1 **a** Typical interaction geometry for two Gaussian laser-beam interferometry; **b** illustration of various phase errors (translational errors: Δx, Δy, Δz, and angular errors: tip θ_x, tilt θ_y, in plane rotation θ_z, and groove period error: ($d_1 - d_2$) of a tiled two-gratings assembly

Z_R ($=\pi W_o^2/\lambda$ is the Rayleigh range and last term in exponent is position dependent Guoy phase shift.

For two Gaussian laser beams propagating at respective angles, θ_i and ϕ_i (subscript $i=1,2$; corresponds to two beams) with respect to x- and y-axes defined in the Fig. 1a, the resultant two-dimensional interferogram $F(x,y)$ at given propagation distance z may be expressed as

$$F(x,y) = I_1\left(x_1,y_1,z_1\right) + I_2\left(x_2,y_2,z_2\right)$$
$$+ 2\sqrt{I_1\left(x_1,y_1,z_1\right)I_2\left(x_2,y_2,z_2\right)}\cos(\varphi 1(x1,y1,z1)$$
$$- \varphi 2(x2,y2,z2)) \quad (2)$$

where x_i, y_i, and z_i may be expressed as

$$x_i = x \cos\theta_i + z \sin\theta_i;$$
$$y_i = -x \sin\theta_i \sin\phi_i + y \cos\phi_i + z \cos\theta_i \sin\phi_i \quad (3)$$
$$z_i = -x \sin\theta_i \cos\phi_i - y \sin\phi_i - z \cos\theta_i \sin\phi_i$$

The parameters $I_1(x_1,y_1,z_1)$, $I_2(x_2,y_2,z_2)$ and $\varphi_1(x_1,y_1,z_1)$, $\varphi_2(x_2,y_2,z_2)$ are the intensities (E.E*) and the phases (term in second exponent of Eq. 1) of two beams, around interaction region as shown in the Fig. 1a. From Eqs. (2) and (3), it is clear that interference fringes may be formed and fringe spatial frequencies shall be governed by the respective angles, θ_i and ϕ_i, the respective beam radii and curvatures of beam phase fronts in general. Local fringe spacing and inclination (magnitude and sign) can be determined by equating differential spatial phases of the two beams to integer multiple of 2π. Under plane wave approximations, straight line fringes are formed with spatial frequencies, along x and y axes related to beam overlap angles (θ_1, ϕ_1) and (θ_2, ϕ_2), as

$$f_x^c = \frac{\left(\sin\theta_2 \cos\phi_2 - \sin\theta_1 \cos\phi_1\right)}{\lambda};f_y^c = \frac{\left(\sin\phi_2 - \sin\phi_1\right)}{\lambda}$$

and are useful in many applications such as diagnostics tool for active locking of any tiled optical surface. In such a case, an interferogram is formed between a reference and reflected or diffracted beam from a tiled optical surface, e.g. tiled grating assembly. The phase function of planner tiled surface can be expressed as $h(X,Y)=kZ+$constant, where coordinates (X, Y, Z) can be determined using transformations of the Cartesian coordinates for the given values of tip angle (θ_x), tilt angle (θ_y), in-plane rotation (θ_z), longitudinal piston (Δx) and lateral piston (Δz) errors as shown in the Fig. 1b. Lateral piston along y axis is ignored, as precise control is not required in case of tiled grating assembly. For a tiled grating assembly, an effective tip [θ'_x], effective tilt [θ'_y] and effective translational errors [$\Delta z'$] for interferometry between reference and diffracted beam are expressed, using equations $\sin(\alpha+\theta_y)+\sin(\beta-\delta\theta_y)=N\lambda/\cos\theta_z$ and $\sin\theta_x - \sin\theta'_x=N\lambda$ $\sin\theta_z$ along horizontal and vertical directions, as

$$\theta'_x = \theta_x - (\sin\alpha + \sin\beta)\theta_z; \text{ and}$$

$$\theta'_y = -(\cos\alpha/\cos\beta)\theta_y + \lambda\Delta N/\cos\theta_z; \qquad (4)$$

$$\Delta z' = (\cos\alpha + \cos\beta)\Delta z + (\sin\alpha + \sin\beta)\Delta x$$

where parameters α and β are the angles of incidence and diffraction, respectively and are much larger than angular errors; the parameter ΔN is the groove density mismatch with N being the groove density. Relative contributions in each term shall depend on sign and magnitude of differential angles, positions and groove density of a tiled grating assembly. It is clear from the Eq. (4) that using interferometry, one can estimate three parameters, i.e. effective tilt, tip and piston error for given tilt, tip, in-plane rotation, longitudinal and lateral pistons, and groove density errors. In the absence of groove density mismatch, the differential tilt angle can be estimated easily. However, in-plane rotation error is paired with tip error, and therefore these two are also difficult to estimate and correct by actuating tip of tiled grating assembly alone. However, it is straightforward to differentiate in-plane rotation error with tip by simultaneous monitoring of the far field of the diffracted and reflected beams as focal spots due to diffraction and reflection shall appear at different planes. For an interferogram recorded for an object with surface distribution h(x, y) with respect to the reference planer object (such as flat mirror), function h(x, y) can be obtained from estimated $\Delta\varphi$ (x, y) as

$$h(x, y) = \frac{\lambda}{2\pi}\frac{\Delta\varphi(x, y)}{m} \qquad (5)$$

where parameter m is a constant depending upon the geometry of the experimental setup and equals to 2 in a double-pass measurement setup. It is further mentioned here that in the case of tiled grating assembly, one is interested to retrieve information on relative beam angle by estimating peak spatial carrier frequencies and piston using suitable calibrations defined in Eqs. 4 and 5.

Figures 2 and 3 show typical theoretical interferograms, generated between a referenced beam propagating at angles, θ_r and ϕ_r and two halves of the beam—diffracted from movable grating (MG) and fixed gratings (FG) of TTGA (kept at Littrow configuration in the present setup)—propagating at angles, θ_{t1}, ϕ_{t1} and θ_{t2}, ϕ_{t2} relative to x- and y-axes, respectively. While Fig. 2 shows typical interferograms for no or large amounts of phase errors in TTGA, Fig. 3 depicts typical interferograms for small amounts of phase errors of TTGA. Corresponding power spectrum in each example is also shown in the Figs. 2 and 3.

While the parameters θ_r, ϕ_r and θ_{t1}, ϕ_{t1} are fixed for a given configuration, θ_{t2} and ϕ_{t2} are variables to control and correct differential tip and tilt angles of tiled optical surface. While spatial frequencies of the interferogram in the two halves are governed by the relative beam cross-over angles ($\Delta\theta_{ti} = \theta_r - \theta_{ti}$ and $\Delta\phi_{ti} = \phi_r - \phi_{ti}$) of the
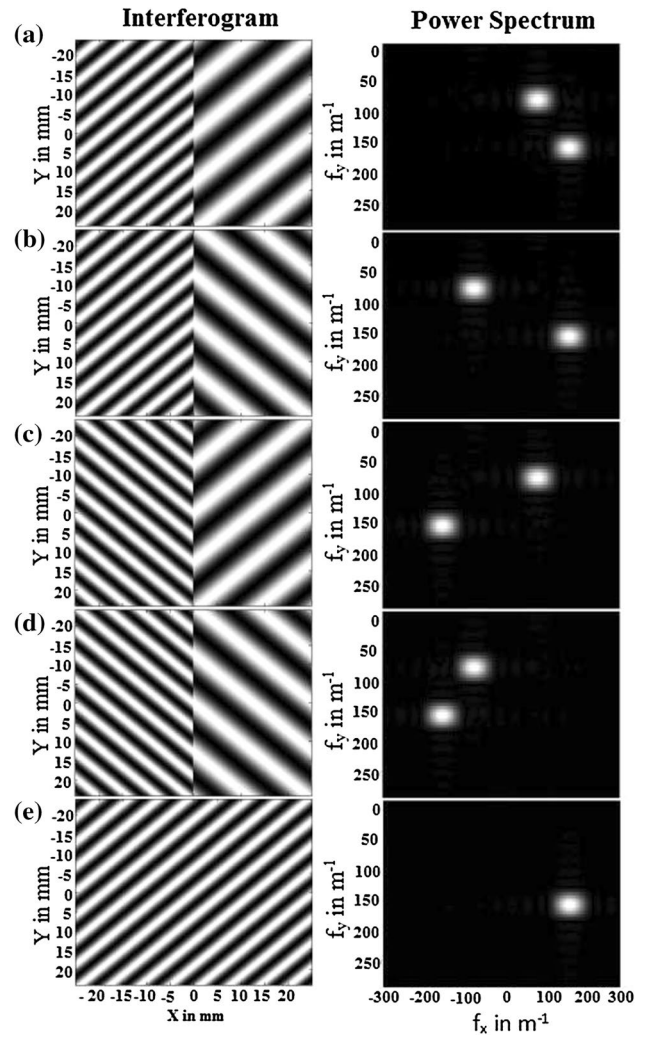

Fig. 2 Theoretical interferogram (*left*) and corresponding upper half of the Fourier spectrum (*right*) between the reference and diffracted beams from TTGA for different values of differential angles [$\Delta\theta_{t1}$, $\Delta\phi_{t1}$, $\Delta\theta_{t2}$, $\Delta\phi_{t2}$] in μrad: **a** ± [+100, +100, +50, +50] or ± [+100, +100−50, −50]; **b** ± [+100, +100, +50, −50] or ± [−100, −100, −50, +50]; **c** ± [+100, −100, +50, +50]; or ± [+100, −100, −50, −50]; and **d** ± [+100, −100, +50, −50] or ± [−100, +100, −50, +50]; and **e** ± [+100, +100, +100, +100]

reference and diffracted beams from the tiled surface and are arbitrary, the differential angles ($\Delta\theta_t = \theta_{t1} - \theta_{t2}$ and $\Delta\phi_t = \phi_{t1} - \phi_{t2}$) constitute the phase profile of the tiled planner optical surface that needs to be estimated. To illustrate the effects of magnitude and sign of relative beam cross-over angles on interferogram for TGA, different values of θ_{t1}, ϕ_{t1} and θ_{t2}, ϕ_{t2} relative to the reference beam have been chosen, which result in identical orientation of fringes in the two halves of the interferogram of TTGA. In such cases, it is not possible to generate adequate control using interferogram alone. Knowledge of magnitude and sign of beam cross-over angles relative to the reference beam is needed and is easily obtained by

Fig. 3 Theoretical interferogram (*left*) with spatial carrier frequency of 158 m^{-1} in *y*-axis and corresponding power spectrum (*right*) of apodized interferogram (*inset*) for smaller values of the phase errors: **a** pure tip error of 10 μrad; **b** pure tilt error of 10 μrad; **c** Tip and tilt errors of 10 μrad each; and **d** pure piston error of π. Line-outs of interferograms are also depicted to show discrimination between translational and angular errors. While full power spectrum, for the example given, is shown in **b** and **d**, the negative frequencies along the *y* axis are ignored in power spectra shown in **a** and **c** for a clearer illustration of spatial frequencies. A *white line* in power spectrum shown in **b** is also drawn to enable easier visualization in shifting of spatial frequencies due to the tilt error. *Top-left* inset in power spectrum of **a** shows apodized interferogram
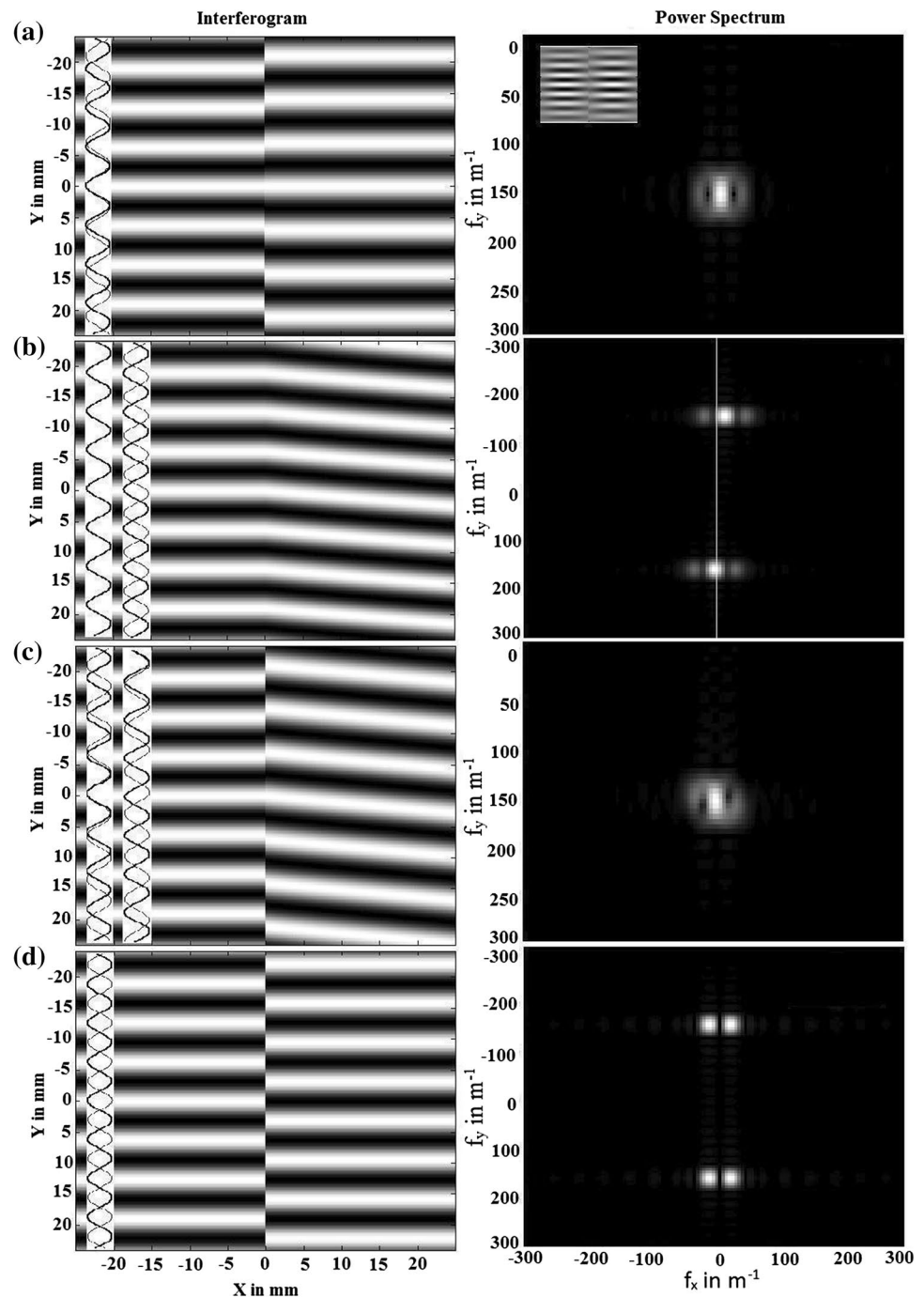
monitoring the reference beam relative to the diffracted or reflected beam from TGA. Next, it is seen from the Fig. 2 that tip and tilt errors of the tiled surface can be visually detected and easily corrected by comparing peak spatial frequencies (and hence fringe spacing and orientation) in the two halves of the interferogram.

Next, for smaller positional and angular phase errors, image processing of two halves of an interferogram is highly desirable to estimate spatial carrier frequencies and hence fringe spacing and orientation. In such a case, power

spectrum of the full interferogram also becomes quite sensitive to phase errors and may be taken as visual indicator to detect phase errors, as illustrated in the Fig. 3a–c. This is much more evident in the case of pure piston error, as depicted in the Fig. 3d. For a pure piston phase error of π, the power spectrum of interferogram is splited into two halves with equal intensity. The intensity ratio of the two lobes changes periodically, and the ratio of two lobes is taken as indicator for piston error. It is clearly seen from the Fig. 3 that constant phase slip is an example of pure

piston shown in Fig. 3d, while spatially varying phase slip is an example of tip/tilt error as shown in Fig. 3a, b. Fig. 3c shows an example of simultaneous presence of tip and tilt errors.

Next, it is mentioned that piston error can be estimated and minimized either by maximizing the ratio of fundamental to second harmonic carrier frequency using a Fourier transformation of product of two signals (i.e. line-outs of interferograms at the extreme right of the first half and at the extreme left of the second half, as shown in the left side of Fig. 3a–d) or by estimating phase shifts of two signals using peak fringe spatial locations. Line-out interferograms at the extreme right of the first half and the extreme right of the second half are also shown in Fig. 3b, c for tilt error, as former pair of line-outs cannot be used to detect this error. It is clear from Figs. 2 and 3 that spatial carrier frequencies of the two halves of the interferogram can be estimated with high precision, and reducing the difference between the two is necessary to achieve the minimum differential tip and tilt errors of TTGA. It is worthy to mention here that for phase locking of planner TTGA, one is interested in estimating peak spatial carrier frequencies by ignoring the distribution of spatial frequencies, and hence the relative errors in the beam pointing in the diffracted and reflected beams from TTGA.

The effects of thresholding, apodization, and padding in estimating spatial carrier frequencies from a noisy interferogram are illustrated by the example given in Fig. 4. It may be noted from this figure that for a noise-free interferogram, errors in the spatial carrier frequencies are less than 1% without apodization and padding (Fig. 4a), which reduce to ~0.01% upon apodization and with padding factor of 4 (Fig. 4b) for a power threshold of 10%. The error in the spatial carrier frequencies remains less than 1% even for a phase noise with standard deviation of $3\lambda/4$ with mean of 0 with apodization and with padding factor of 4 for threshold of 80% (Fig. 4c). It is clear from these examples that thresholding, apodization and padding help to improve precision in the estimation of spatial carrier frequencies. In this example, where spatial carrier frequencies are along both x- and y-axes (example shown in the Fig. 4), both tip and tilt errors shall be affected by the ratio of the respective spatial carrier frequency to the sampling frequency. In case, when spatial carrier is along one direction, for example, along y-axis alone as shown in Fig. 3, it is the tip error which is the most affected by the ratio of actual spatial frequency to sampling frequency limit for spatial carrier. In summary, the angular error decreases with the increasing padding factor and is much smaller when actual fringe frequencies approach towards multiple or half integer multiple of the sampling frequency limit set by the detector for an apodized interferogram. Therefore, fringe frequencies of the interferogram are chosen such that these are multiple

or half integer multiple of the sampling frequency limit. The padding of an interferogram may be understood as extrapolating the fringe pattern so as to effectively improve the angle estimation and is taken as a trade-off between desired accuracies and computational time. Next, error in estimating the spatial carrier frequencies increases with the increase in intensity or phase noise. However, the use of thresholded power spectrum substantially reduces the error in the estimation of spatial carrier frequencies.

3 Experimental setup and results

Figure 5 shows a typical experimental setup to demonstrate a prototype of an active phase locking of TTGA consisting of two gratings 110 mm × 80 mm × 10 mm, each with a groove density of ~1740 lines/mm. TTGA is illuminated at Littrow configuration by a well-collimated beam of ~50 mm diameter (estimated full angle divergence of ~16 µrad) from a He-Ne laser ($\lambda = 632.8$ nm) coupled with suitable beam expander and a beam splitter. An interferogram between the reference and diffracted beam from TTGA is generated and recorded using an eight-bit CCD camera (pixel size: 8.6 µm × 8.3 µm) with a suitable beam de-magnifier as shown in the Fig. 5. Far-field distribution of the reflected and diffracted beams from a TTGA together with far field of a reference beam are recorded using another CCD with the help of suitable beam splitter and mirror combination as depicted in the Fig. 5. For a perfect phase locking of two gratings, difference in the groove density of the two gratings may also result in angular mismatch between two halves of the diffracted beam and hence focal spot splitting (or modulation in the far-field beam profile) of otherwise single focal spot of the diffracted beam. Present setup also helps to study and compensate for a slight mismatch if any between groove densities of two gratings with a differential tilt angle, and a single focal spot of the diffracted beam from the tiled grating assembly is achieved. The accuracies in determining the groove density errors or other phase errors depend on wave front quality of the incident laser beam and optical aberrations.

While one grating of TTGA is mounted using additional adapter on two nanometric actuator-driven mirror mount 8821 kept on a linear translational stage with nanometric actuator 8303 V to achieve tip, tilt and longitudinal piston error correction, the other grating is placed on an another mount with a nanometric actuator 8303 V for in-plane rotation error correction. All four nanometric actuators are NewFocus make and controlled using NewFocus controller 8752 interfaced with a personal computer. The two analog signals from two CCDs (Watec 902B) are digitized using national instrument video frame grabber card NI1410
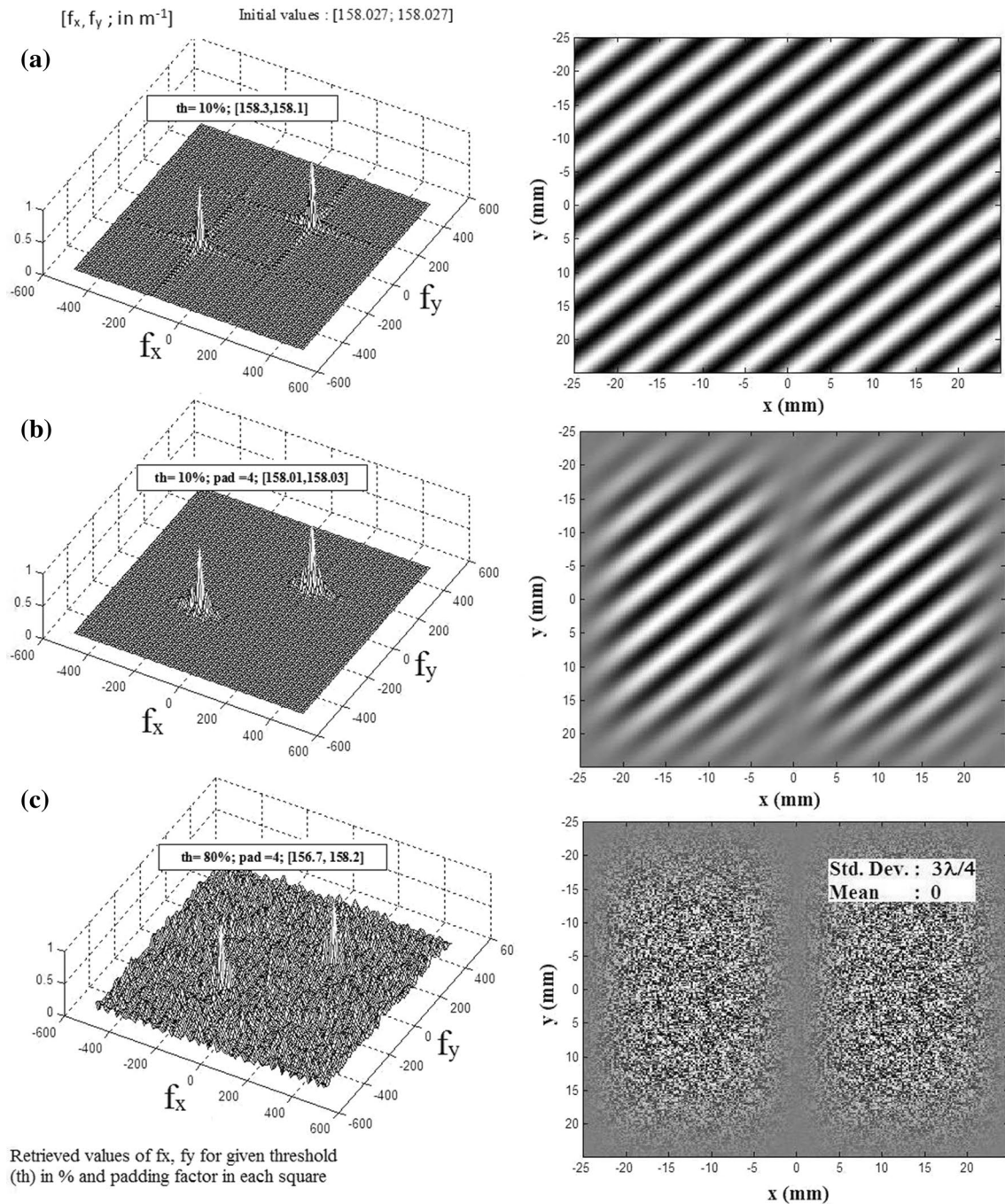
Fig. 4 Power spectrum corresponding to a theoretical interferogram with spatial carrier frequencies of 158 m^{-1} in x- and y-axes under different conditions: **a** no apodization and noise-free interferogram; **b** apodized interferogram with no intensity or phase noise; and **c** apodized interferogram with a random phase noise with standard deviation of $3\lambda/4$ and zero mean value1

through multiplexer A6822 to allow processing of interferogram and far-field intensity distribution of the reference beam, reflected and diffracted beams from TTGA to derive necessary controls for four nanometric actuators in order to correct tip, tilt, longitudinal piston and in-plane rotation errors.

In the present case, phase locking is achieved in following steps. First, spatial carrier frequencies are estimated from both halves of an interferogram, and error is corrected using tip/ tilt actuators. Then in-plane rotation errors between the two gratings are estimated and controlled using a third nanometric actuator by simultaneous monitoring
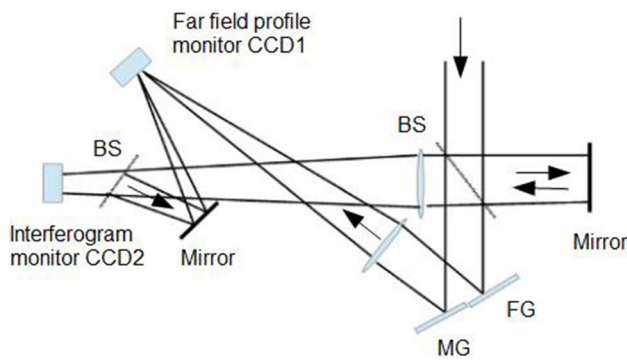
Fig. 5 Typical experimental setup for estimation and correction of various phase errors of the tiled two-grating assembly (TTGA)

the peak positions of the far-field intensity distribution of the diffracted and reflected beams from TTGA. To achieve this, a diffracted and a reflected beam from TTGA and a referenced beam are focused on to a single CCD camera using a long focal length lens to meet the required accuracies in the angle measurements. Once in-plane rotation is corrected, tip and tilt errors are corrected again using a feedback loop. Once tip, tilt and in-plane rotation errors are corrected, TTGA is phase locked in such a way that phase errors due to piston are minimized using a fourth nanometric actuator. Finally, a mismatch in the groove density of the two tiled gratings is estimated by analyzing focal spot of a diffracted beam and suitably locked by compensating through tilt error to achieve single focal spot of diffracted beam for a TTGA.

Figure 6 shows typical experimental interferograms of TTGA (I), line outs used to retrieve piston error at extreme right and extreme left edge of the first and the second halves of interferogram (II), far-field profiles of the diffracted and reflected beams from TTGA (III), the combined power spectrum of individual interferograms (IV), and the power spectrum of full interferogram (V) under different conditions of phase-locked and non-phase-locked TTGA. Interferogram shown in I is cropped for clearer depiction of fringes with typical spatial carrier frequency in range 1.1–1.5 lines per mm in both the halves. Various power spectra shown in Fig. 6 are not to scale. Figure 6a shows an example of non-phase-locked TTGA with tip, tilt, in-plane rotation and piston errors. Differential tip and tilt errors are estimated to be 106, 143 μrad from the estimated central spatial carrier frequencies of the interferogram. In order to compare these values, the tip and tilt errors are also estimated from far-field spatial profiles of the diffracted and reflected beams. While tip and tilt errors are estimated to be 101, 133 μrad from the diffracted focal spot, values for tip and tilt errors are estimated to be 74, 130 μrad from the reflected far-field spatial profiles, respectively. Differences in the tip errors obtained using the diffracted and reflected

spots are attributed to in-plane rotation. Figure 6b depicts a phase-locked TTGA with differential tip, tilt, in-plane rotation errors of less than 10 μrad and differential piston error less than 50 nm estimated using interferometry. Further, it may be seen that single far-field beam profiles are not achieved in the diffracted and reflected beams, even when interferometry data show a phase-locked condition. The separation in the two lobes of the spots in the diffracted and reflected beams along horizontal direction is attributed to either the groove density errors of the two gratings or optics/ beam aberrations. The CCD of far-field profile was placed at best focal condition for both the reflected and diffracted beams. In order to achieve single diffracted spot as shown in Fig. 6c, a tilt error of ~30 μrad was introduced after conditions corresponding to example shown in Fig. 6b have been achieved. Figure 6d corresponds to phase-locked condition but with introduction of piston error of π after conditions corresponding to the example shown in Fig. 6c. In this case, one may see that the far-field profiles of the diffracted beam mimic that of computed power spectrum of full interferogram and may be useful as a visual indicator for piston like errors.

To demonstrate that single interferogram alone recorded using the reference and diffracted beams cannot distinguish in-plane rotation and tip error, two examples of non-phaselocked TTGA with known in-plane rotation error and in-plane rotation error corrected by equivalent tip error are given in Fig. 6e, f, respectively. The estimated value for effective tip from interferogram is ~381 μrad, and this compares well with the estimated in-plane rotation error from the recorded far-field spatial profiles of the diffracted and reflected beams. It is clear from Fig. 6f that single interferogram cannot be taken as an indicator for a phase-locked gratings. This is visually seen by looking at mismatch between the planes of reflection and diffraction in the two examples, i.e. Figure 6e, f. The tip error of ~380 μrad is estimated from the far-field profile of the reflected beam. Phase locking of the TTGA has also been tested in standard common path Fizeau interferometer configuration with added diagnostics for far-field profiles of the reference, reflected and diffracted beams from TTGA. For laser pulse compressor of 50 TW class hybrid Nd:glass laser, a large aperture interferometry using highly broadband light source shall be carried out along with far-field diagnostics using low power monochromatic beam to correct various errors in a global optimization in a way that both spatial and temporal characteristics of ultrashort pulsed laser beam are maintained. Further, correcting errors with a high precision to all tiled grating assembly shall not be required.

The accuracies in estimating the tip, and tilt errors from interferometry are dictated by the accuracies in estimating the peak spatial carrier frequencies. The size of full interferogram used for analysis is kept at 512×512 pixels, and
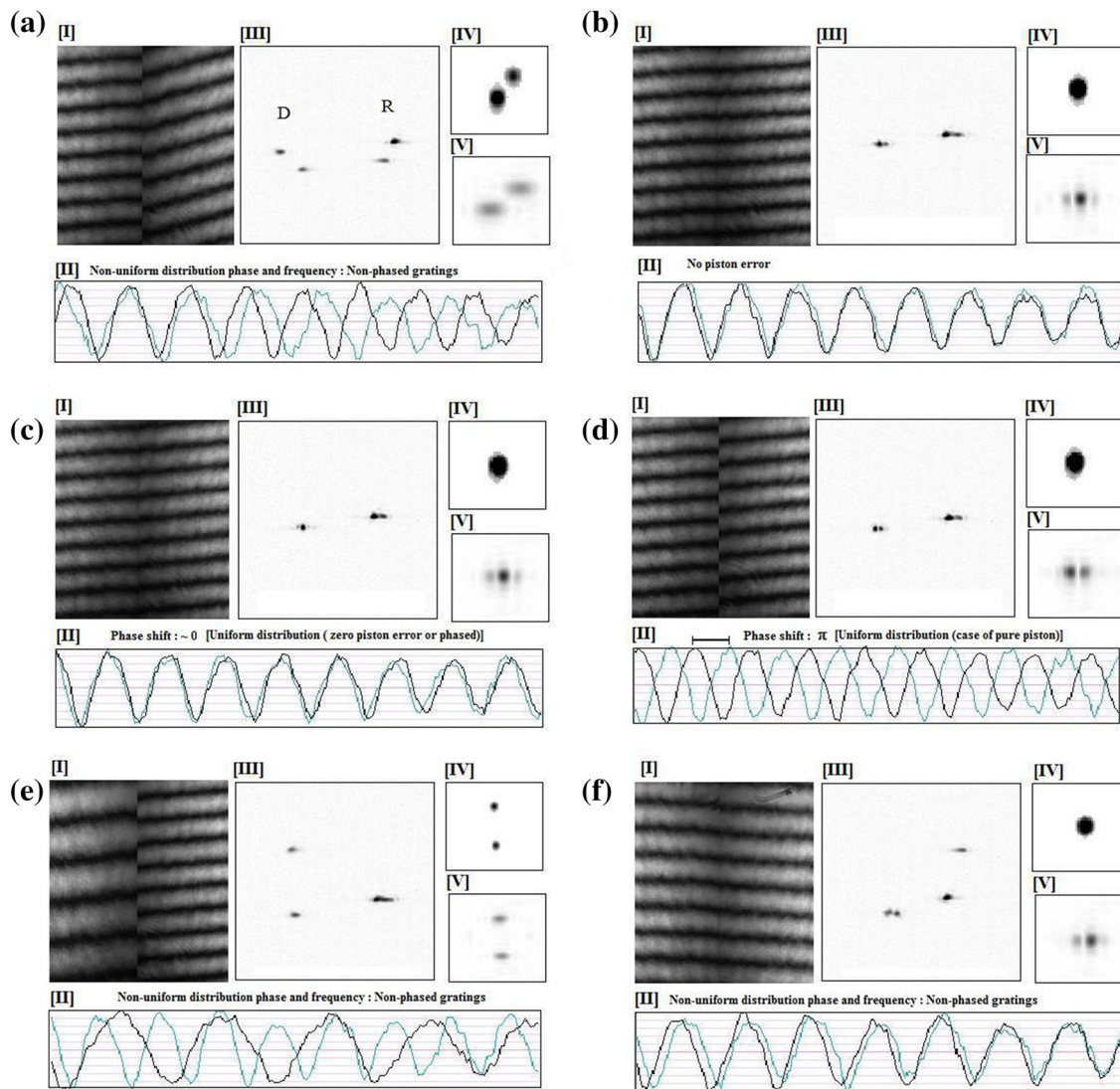
Fig. 6 Experimentally observed interferogram (*I*), line outs used to retrieve piston error at the extreme right and the extreme left edges of the first and the second halves of interferogram (*II*), far-field distribution of the diffracted and reflected beams (*III*), combined computed power spectrum of individual interferograms (*IV*), and computed power spectra of full interferogram (*V*) for different conditions of TTGA: **a** with tip, tilt, in-plane rotation and piston errors; Estimated errors (tip,tilt) using interferogram, diffracted (*D*), reflected (*R*) far-field profile are (106 μrad, 143 μrad), (101 μrad, 133 μrad), and (74 μrad, 130 μrad), respectively. Differences in the tip errors obtained using the diffracted and reflected spots are attributed to in-plane rotation; **b** phase-locked gratings with differential tip, tilt, in-plane rotation errors less than 10 μrad and piston errors less than 50 nm; and **c** phase-locked grating with intentional tilt error of ~30 μrad after conditions of TTGA shown in **b** are achieved to obtain single diffracted spot as depicted in the left side of sub-figure (*II*); **d** phase-locked gratings with piston error of π after conditions of TTGA shown in **c** are achieved; **e** Non-phased gratings with in-plane rotation error of 381 μrad to achieve near single reflected spot; and **f** Non-phased gratings with tip error of 300 μrad compensated with in-plane rotation to achieve near single diffracted spot. Power spectra shown are not to scale

the spatial frequency resolution [$f_{res} = (\delta x N)^{-1}$] is ~48 m^{-1} for an effective pixel size (δx) of ~40μ m. This corresponds to an angular resolution [$\sin^{-1}(\lambda f_{res})$] of ~30 μrad, which can be improved by, reducing effective pixel size, extrapolating the interferogram and with sub-pixel spatial frequency estimation as demonstrated in the present case. The piston errors are estimated using line outs at extreme right and extreme edge of the first and the second halves of interferogram in two ways: one by estimating the peak fringe locations directly and the other by calibrating the ratio of power spectrum at fringe and twice the fringe frequency of the product of the two line outs, respectively. In case of estimating the peak spatial fringe locations, the accuracy in longitudinal piston is estimated to be less than 5% of the

wavelength and is governed by the accuracy to which fringe peak location is estimated relative to extent of one fringe and is self-calibrating as the extent of one fringe being equal to laser wavelength. Next, the angular accuracies in far-field profiles of the diffracted and reflected beams from the TTGA are estimated to ~5 μrad for one CCD pixel and using a convex lens with focal length of 1.5 m. Coupled with sub-pixel centroid detection and analyzing far-field profile of the two spots separated by tip angle, the actuator-limited differential angular errors of ~1 μrad (corresponding to ~50 nm over full grating aperture), which is smaller than diffraction-limited angular accuracies of ~16 μrad. Such accuracies are sufficient to achieve a single-diffracted focal spot for laser beams with natural beam divergence of ~10 μrad either in the case of using tiled grating assemblies, e.g. POLARIS (10–11) in Germany, OMEGA-EP in USA (8,17–18) or in the case of using multiple-beam phasing, e.g. PETAL in France (13–15) for high-energy laser pulse compression.

Figure 7 shows closed-loop variations of differential tip, tilt and piston errors for a TTGA with and without locking under different environment conditions. It may be noted that differential angular errors are locked to within ±5 μrad, while the estimated piston was locked below $\lambda/20$ (piston error is magnified by 50× in Fig. 7 for a clearer visualization; $\lambda = 633$ nm) using interferometric data as control for tip, tilt and piston errors. Estimated piston error does not account for the angle of incidence correction given by Eq. (4) and is for a fixed unknown value of lateral translation Δx. Ambiguities in longitudinal Δz and lateral translation Δx have not been removed in the present case and may not be necessary in pulse compression and while maintaining single diffracted focal spot. Next, it may be mentioned
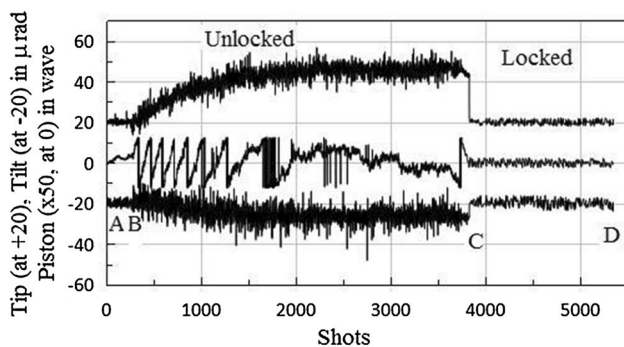
that lateral translation may affect the ability to focus the beam and may lead to generation of temporal satellites due to spectral clipping. Relative contribution is governed by the pulse compression design and the beam parameters. In any case, lateral separation between the tiled gratings is kept to be as minimum as possible before precise alignment of tiled gratings is attempted using active feedback loop. Although the in-plane rotation error is corrected using nanometric actuator to desired accuracies, there is no active feedback loop for in-plane rotation error in the present case. Further, it may be worthy to mention here that in-plane rotation actuation is applied to one grating of TTGA, while tip/ tilt actuation is applied to other grating so as to avoid any cross-talk due to different movements. It is observed that in-plane rotation remains stable for measurements carried out over ~1 h. Moreover, smaller in-plane error shall not affect the temporal pulse compression, and the focal spot intensity distribution is suitably corrected with tip error. It may be mentioned that the refresh rate (time taken to estimate and correct the error) in an active feedback loop depends on several factors, e.g. magnitude of the errors to be corrected and the reliability of the actuator, etc. In the present case, tip and tilt errors are corrected typically within few seconds, while correcting piston error sometimes takes more than a minute. Next, while the piston error is corrected in active loop by translating actuator back and forth with step much smaller than wavelength, there remains some chance that it may cross one fringe due to limited reliability of the actuator and movable grating may drift in either direction leading to different compression lengths but this shall not effect the compressed pulse duration due to larger compression distances and limited range of actuator. Such drifts shall be either controlled using fringe visibility of interferogram recorded with highly broadband source or using translational limit switches in future. In summary, estimating the spatial carrier frequencies and the piston errors from interferogram with a high precision is the backbone of the control algorithm. Any error in estimating them shall directly affect the phase locking of the tiled grating assembly. Multiple level intensities in thresholds of power spectra combined with padding and apodization helps in improving the estimation of the spatial carrier frequencies. Any variation in acquired interferogram due to noise or any other technical issues in image acquisition may also lead to inaccurate estimation of spatial carrier frequencies and hence error in automatic phase control of TTGA. Active phase locking is started after initial optimization is carried out manually and various parameters, e.g. spatial carrier frequency of the interferogram, are suitably chosen.

Fig. 7 Experimentally observed closed-loop variations of differential tip, tilt and piston errors for a TTGA without and with active locking. Unlocked region is from point *A* to point *C* (*A* to *B* minimum disturbances; *B* to *C* with larger disturbances), while locked phase region is from point *C* to point *D*. Tip and tilt error variations are shifted to mark +20 and −20, respectively, and are in μrad; the piston at mark *0* is multiplied by 50 for a clearer visualization

4 Conclusion

In conclusion, experimental studies on a prototype of phase locking of tiled gratings assembly for high-energy pulse compression have been demonstrated with a worst-case precision of sub-50 nm in differential piston and sub-10 μrad in differential tip, tilt, and in-plane rotation errors using four control variables derived from simultaneous monitoring of far-field laser beam profiles and two-dimensional interferometry. Criticalities in various parameters in order to achieve active phase locking of tiled grating assembly are discussed with theoretical and experimental results. The key to achieve higher accuracies in the tip and tilt errors is in the estimation of spatial carrier frequencies with higher precision from a single noisy interferogram and achieved using multiple-level intensity thresholds of a power spectrum of an apodized and padded interferogram. Finally, short- and long-term studies on differential tip, tilt and piston errors have also been demonstrated over 1 h.

References

1. J.D. Zuegel, S. Borneis, C. Barty, B. Legarrec, C. Danson, N. Miyanaga, P.K. Rambo, C. Leblanc, T.J. Kessler, A.W. Schmid, L.J. Waxer, J.H. Kelly, B. Kruschwitz, R. Jungquist, E. Moses, J. Britten, I. Jovanovic, J. Dawson, N. Blanchot, Fusion Sci. Technol. **49**, 453 (2006)
2. G. R. Kumar, Pramana, **73**(1), 113 (2009)
3. S. Banerjee, S. Chen, N. Powers, D. Haden, C. Liu, G. Golovin, J. Zhang, B. Zhao, S. Clarke, S. Pozzi, J. Silano, H. Karwowski, D. Umstadter, Nucl. Instr. Meth. Phys. Res. B **350**, 106 (2015)
4. M. Storm, S. Jiang, D. Wertepny, C. Orban, J. Morrison, C. Willis, E. McCary, P. Belancourt, J. Snyder, E. Chowdhury, W. Bang, E. Gaul, G. Dyer, T. Ditmire, R.R. Freeman, K. Akli, Phys. Plasmas **20**, 053106 (2013)
5. C.M. Brenner, S.R. Mirfayzi, D.R. Rusby, C. Armstrong, A. Alejo, L.A. Wilson, R. Clarke, H. Ahmed, N.M.H. Butler, D. Haddock, A. Higginson, A. McClymont, C. Murphy, M. Notley, P. Oliver, R. Allott, C. Hernandez-Gomez, S. Kar, P. McKenna, D. Neely, Plasma Phys. Control. Fusion **58**, 014039 (2016)
6. W. Leemans, E. Esarey, Phys. Today **62**(3), 44 (2009)
7. T. Zhang, M. Yonemura, Y. Kato, Opt. Commun. **145**, 367 (1998)
8. T.J. Kessler, J. Bunkenburg, H. Huang, A. Kozlov, D.D. Meyerhofer, Opt. Lett. **29**, 635 (2004)
9. J. Bunkenburg, T.J. Kessler, W. Skulski, H. Huang, Opt. Lett. **31**, 1561 (2006)
10. M. Hornung, R. Bodefeld, M. Siebold, M. Schnepp, J. Hein, R. Sauerbrey, M.C. Kaluza, Appl. Opt. **46**, 7432 (2007)
11. M. Hornung, R. Bodefeld, A. Kessler, J. Hein, M.C. Kaluza, Opt. Lett. **35**, 2073 (2010)
12. C. Hernandez-Garcıa, C. Mendez, I. Arias, J.R. Vazquez de Aldana, O. Varela, I.J. Sola, L. Roso, Appl. Phys. B **108**, 773 (2012)
13. N. Blanchot, G. Marre, J. Néauport, E. Sibe, C. Rouyer, S. Montant, A. Cotel, C. Le Blanc, C. Sauteret, Appl. Opt. **45**(23), 6013 (2006)
14. N. Blanchot, E. Bar, G. Behar, C. Bellet, D. Bigourd, F. Boubault, C. Chappuis, H. Coic, C.D. Dupont, O. Flour, O. Hartmann, L. Hilsz, E. Hugonnot, E. Lavastree, J. Luce, E. Mazataud, J. Neauport, S. Noailles, B. Remy, F. Sautarel, M. Sautet, C. Rouyer, Opt. Exp. **18**, 10088 (2010)
15. T. Harimoto, Jpn. J. Appl. Phys. **43**(4A), 1362 (2004)
16. A. Cotel, M. Castaing, P. Pichon, C. Le Blanc, Opt. Express **15**, 2742 (2007)
17. J. Qiao, A. Kalb, M.J. Guardalben, G. King, D. Canning, J.H. Kelly, Opt. Exp. **15**, 9562 (2007)
18. Demonstration of real-time, phase-pocked alignment of tiled gratings for chirped-pulse amplified lasers, Laboratory for Laser Energetics (LLE) Review Quarterly Report **100**, 242 (2004)
19. H. Habara, G. Xu, T. Jitsuno, R. Kodama, K. Suzuki, K. Sawai, K. Kondo, N. Miyanaga, K.A. Tanaka, K. Mima, M.C. Rushford, J.A. Britten, C.P.J. Barty, Opt. Lett. **35**, 1783 (2010)
20. Y. Hu, L. Zeng, Appl. Opt. **46**(28), 7018 (2007)
21. Y. Yang, X. Wang, J. Zhang, H. Luo, F. Li, X. Huang, F. Jing, Opt. Laser Eng. **50**, 262 (2012)
22. Y. Yang, X. Wang, J. Zhang, H. Luo, F. Li, X. Huang, F. Jing, Opt. Eng. **50**, 093601 (2011)
23. A.S. Joshi, M.P. Kamath, A.K. Sharma, M. Raghuramaiah, R.K. Patidar, M.S. Ansari, N. Sreedhar, R. Chandra, C.P. Navathe, P.A. Naik, P.D. Gupta, EPJ Web of Conferences **59**, 08001 (2013)
24. A.K. Sharma, M. Raghuramaiah, R.K. Patidar, A.S. Joshi, P.A. Naik, P.D. Gupta, International symposium on Chirped Pulse Amplification, Laval University, Quebec, Canada Nov. 17–21 (2010).
25. A.K. Sharma, P.A. Naik, P.D. Gupta, Proc. of DAE-BRNS National Laser Symposium (NLS-21), BARC, Mumbai Feb 6–9 (2013)
26. A.K. Sharma, D. Daiya, R.K. Patidar, M. Raghuramaiah, A.S. Joshi, P.A. Naik, P.D. Gupta, International council of ultra intense laser (ICUIL) conference 2012, Romania, Sept 16–21 (2012).
27. Z. Vucic, J. Gladic, Appl. Opt. **44**, 6940 (2005)
28. J. Gladic, Z. Vucic, D. Lovric, Opt. Laser Eng. **45**, 868 (2007)
29. C. Roddier, F. Roddier, Appl. Opt. **26**, 1668 (1987)
30. C. Quan, C.J. Tay, L.J. Chen, Opt. Laser Technol. **39**, 1155 (2007)
31. M. Takeda, K. Mouth, Appl. Opt. **22**, 3977 (1983)